journal of the mechanical behavior of biomedical materials 121 (2021) 104641

Contents lists available at ScienceDirect

Journal of the Mechanical Behavior of Biomedical Materials

journal homepage: www.elsevier.com/locate/jmbbm

Research paper

Time-dependent *in silico* modelling of orthognathic surgery to support the design of biodegradable bone plates

Antoine Vautrin [a,b], Mariska Wesseling [b], Roel Wirix-Speetjens [b], Maria Jose Gomez-Benito [a,*]

[a] Multiscale in Mechanical and Biological Engineering (M2BE), University of Zaragoza, Zaragoza, Spain
[b] Materialise NV, Leuven, Belgium

ARTICLE INFO

Keywords:
Orthognathic surgery
Biodegradable magnesium
Bone fracture healing
Finite element analysis

ABSTRACT

Orthognathic surgery is performed to realign the jaws of a patient through several osteotomies. The state-of-the-art bone plates used to maintain the bone fragments in place are made of titanium. The presence of these non-degradable plates can have unwanted side effects on the long term (e.g. higher infection risk) if they are not removed. Using a biodegradable material such as magnesium may be a possible solution to this problem. However, biodegradation leads to a decrease of mechanical strength, therefore a time-dependent computational approach can help to evaluate the performance of such plates. In the present work, a computational framework has been developed to include biodegradation and bone healing algorithms in a finite element model. It includes bone plates and the mandible, which are submitted to masticatory loads during the early healing period (two months following the surgery). Two different bone plate designs with different stiffnesses have been tested. The stiff design exhibited good mechanical stability, with maximum Von Mises stress being less than 40% of the yield strength throughout the simulation. The flexible design shows high stresses when the bone healing has not started in the fracture gaps, indicating possible failure of the plate. However, this design leads to a higher bone healing quality after two months, as more cartilage is formed due to higher strains exerted in fracture gaps. We therefore conclude that *in silico* modelling can support tuning of the design parameters to ensure mechanical stability and while promoting bone healing.

1. Introduction

Orthognathic surgery is a type of craniomaxillofacial (CMF) surgery performed when a patient presents a malocclusion (over- or underbite) and is most frequently caused by a congenital defect (Naran et al., 2018). It consists of realigning the jaws by performing several osteotomies. Most surgeries include a Le Fort I osteotomy (maxilla), a bisagittal split osteotomy (BSSO) (mandible), and an osseous genioplasty (chin) (Naran et al., 2018). With 10,000 surgeries performed each year in the US (Venugoplan et al., 2012), this type of surgery is relatively common.

After performing the osteotomy, fixation plates are typically used to maintain the alignment of the jaws during the healing period. The standard solution consists of using titanium plates that the surgeon bends during the surgery to the desired shape. The plates can also be patient-specific. In this case, their design is generated during virtual surgical planning, a method that is increasingly being used for this type of surgery. A CT scan of the patient is used to create a 3D model of the patient's anatomy, which is then used to define the osteotomy plane and reposition the bone segments (Naran et al., 2018). Patient-specific cutting guides and bone plates are generated from this model. They are 3D-printed and therefore possess stronger mechanical properties as they do not undergo permanent plastic strains (Schouman et al., 2015).

Once the bone has healed, two options are available: either a removal surgery is performed or the plates remain in the patient's body. Plates removal entails an additional cost and a risk of infection during the second surgery. However, several problems can arise if they are not removed. From an aesthetic point of view, the plates can be visible and/or can be felt by palpation. Moreover, titanium does not degrade in the human body, and despite its good biocompatibility, leaving an implant for a long time span can be potentially harmful (e.g. increased infection rate, stress shielding) especially given that this surgery is usually performed on young patients (Sukegawa et al., 2018).

Bioresorbable materials represent a possible solution to this problem while saving the cost of a removal surgery. PLLA (poly-L-lactic acid) plates and screws are already commercially available for CMF applications (Inion CPS, Biosorb PDX) (Buijs et al., 2012). However, polymers exhibit a lower strength than titanium and cannot be used for load-bearing applications. Magnesium (Mg) is a biodegradable material with

* Corresponding author.
E-mail address: gomezmj@unizar.es (M.J. Gomez-Benito).

https://doi.org/10.1016/j.jmbbm.2021.104641
Received 31 March 2021; Received in revised form 1 June 2021; Accepted 5 June 2021
Available online 9 June 2021

good mechanical strength but has a relatively fast degradation rate. Using bioresorbable materials makes implant design more challenging because good understanding of its mechanical properties over time is required (Byun et al., 0000).

After the surgery, bone healing occurs in the resulting fracture gaps. During the healing period, the load sharing mechanism between the fracture gaps and plates evolves (Gómez-Benito et al., 2006). The mechanical strength of a biodegradable plate will decrease over time therefore considering its initial properties is not sufficient to evaluate its performance. The plates should be strong enough to support the load until the fracture gaps are sufficiently healed to be able to transmit the mastication loads. Thus, they must maintain sufficient mechanical properties during this healing period. The performance of a given plate design will depend on the biodegradation rate of the plate material, the bone healing process, and the loads applied to the system.

In silico models allow to gain more insights into clinical cases by applying physiological loads, i.e. masticatory loads, which is not achievable experimentally. It also allows to easily change or tune the parameters of the model and observe their influence on the outcome of the surgery. To the best of our knowledge, there are no commercially available *in vitro* devices for this application. Therefore, an *in silico* model could be used to determine the feasibility of medical devices. Computational modelling of bone healing has been extensively described in the literature (Perren and Rahn, 1980; Perren, 2002; Gómez-Benito et al., 2005; Borgiani et al., 2017; Zhao et al., 2018; Alierta et al., 2014) and numerical algorithms of Mg degradation have been developed recently (Gastaldi et al., 2011; Grogan et al., 2011).

Several studies modelled the outcome of different surgeries on the mandible. For instance, Zheng et al. (2019) developed a static FE model of a patient who has undergone mandibular reconstruction in order to evaluate the muscular functionality after this surgery. Wu et al. (2020) performed a topological optimization of bone plates for the same type of application. They considered the case of a bone graft and included a bone remodelling algorithm, the objective of the optimization being the maximization of bone density. The study of Boccaccio et al. (2008) focused on tissue differentiation during mandibular distraction. Thus, computational models of the mandible including bone healing algorithms have been developed, but they have been focusing on non-degradable fixation systems. On the other hand, combined models of biodegradation of fixation plates with bone healing have already been developed for long bones (Mehboob and Chang, 2015; Ma et al., 2018) but not for CMF applications.

In the present work, a finite element (FE) model has been created to evaluate the outcome of a BSSO surgery. A time-dependent approach has been adopted to model the evolution of bone healing and plate biodegradation and their opposite effects on the mechanical strength of the plates. Therefore, this model can be used to compare the performance of different plate designs through time.

2. Material and methods

In order to evaluate the feasibility of using bioresorbable magnesium bone plates for orthognathic surgery, both plate biodegradation and bone healing have to be taken into account. The loss of structural integrity due to biodegradation has to be compensated by the bone healing. Thus, modelling these two processes simultaneously allows us to estimate the evolution of the system. The integration of these algorithms is described on Fig. 1.

2.1. Biodegradation model of magnesium

Numerical models describing the biodegradation of magnesium have been developed with a focus on coronary stents (Gastaldi et al., 2011; Grogan et al., 2011), as it is currently one of the main applications of Mg as a biomaterial. Phenomenological models have been considered here in order to reduce the computational cost.

A phenomenological model of uniform corrosion has been developed by Gastaldi et al. (2011). Grogan et al. (2011) adapted this model to describe pitting corrosion, which is observed experimentally in the case of magnesium. It is an extremely localized form of corrosion where small holes grow in the surface of the material. Both uniform and pitting corrosion models have been calibrated and compared to experimental results (Grogan et al., 2011), where the loss of mechanical strength of the specimens was better predicted by the pitting corrosion model.

This model is based on the continuum damage theory and describes the effective stress tensor ($\tilde{\sigma}_{ij}$) as follows:

$$\tilde{\sigma}_{ij} = \frac{\sigma_{ij}}{1 - D} \tag{1}$$

where D a scalar damage parameter and σ_{ij} is the Cauchy stress tensor. The evolution of the damage parameter D is given by:

$$\frac{\partial D}{\partial t} = \frac{\delta_U}{L_e} \lambda_e k_U \tag{2}$$

where k_U is a corrosion kinematic parameter, δ_U is the material's characteristic length, L_e is the element's characteristic length and λ_e is a dimensionless pitting variable accounting for the heterogeneity of the corrosion process. The material's characteristic length corresponds to the alloy's average grain size. Each element belonging to the exterior surface is assigned a random value of λ_e generated with a Weibull distribution-based random number generator. The Weibull probability density function is given by:

$$f(u) = \gamma u^{\gamma - 1} e^{-u^{\gamma}} \tag{3}$$

where $u \geq 0$ and $\gamma > 0$, γ being the distribution shape factor. In the case of isotropic elasticity, the Young's modulus of the plate (E_p) can be expressed as a function of the damage parameter (D) and of the initial Young's modulus of Mg (E_{p0}):

$$E_p(\boldsymbol{x}, t) = E_{p0}(1 - D(\boldsymbol{x}, t)) \tag{4}$$

At the start of the analysis, corrosion occurs to the elements belonging to the surface of the object. When an element is completely corroded ($D > 0.99$), a very low Young modulus ($E_p = E_{p0}/100$) is attributed to this element and the corrosion is activated in the neighbouring elements. It is not removed to avoid computational instability. A fraction of its pitting variable is transmitted to the neighbouring elements such that:

$$\lambda_e = \beta \lambda_n \tag{5}$$

where λ_e is the pitting variable of the neighbouring elements, λ_n is the pitting variable of the degraded element and β is a dimensionless parameter driving the pit growth evolution.

2.2. Bone healing algorithm

The bone healing algorithm described here is adapted from the model developed by Alierta et al. (2014). It is based on the concept of "biological fixation" first described by Perren (2002). This model was originally defined for a cohesive contact behaviour but has been generalized here to isotropic elasticity. The main variable of the model is the union degree (α) which defines the temporal evolution of the stiffness for each point ($\boldsymbol{x}$) of the fracture gap as:

$$E_g(\boldsymbol{x}, t) = E_{g0} \cdot \alpha(\boldsymbol{x}, t) \tag{6}$$

where E_{g0} is the Young's modulus of immature bone, and E_g is the current Young's modulus of the element. The union degree represents

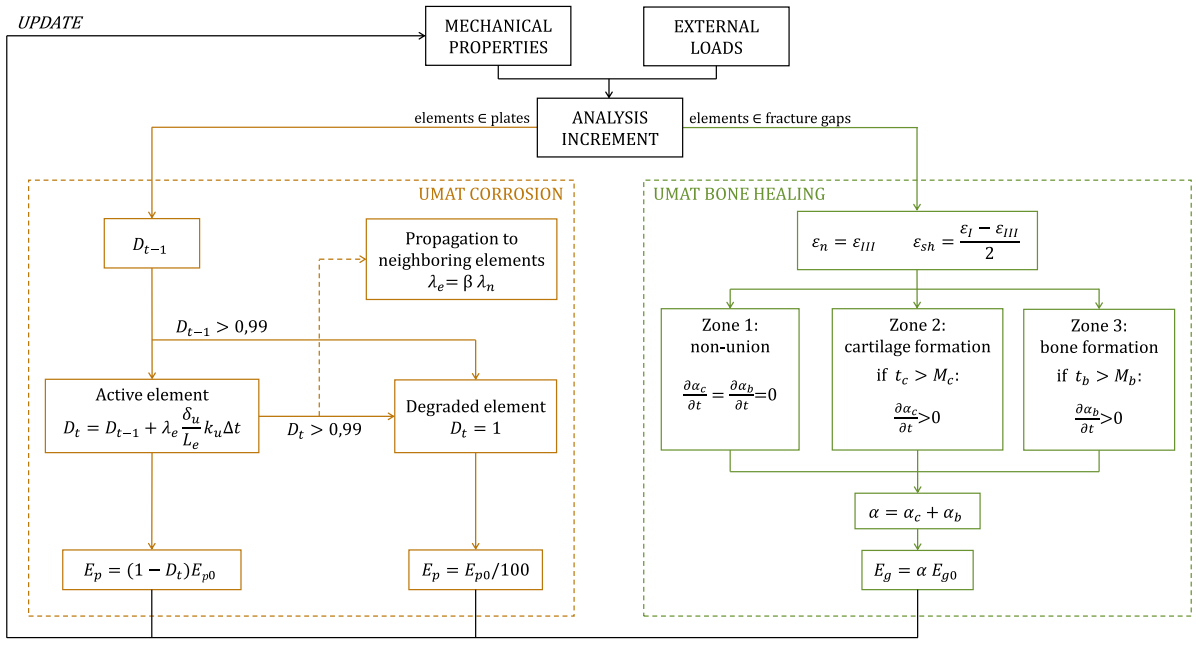

Fig. 1. Flowcharts of the algorithms used in the UMAT subroutines corresponding to corrosion and bone healing.

the ratio between the current value of stiffness and the stiffness of immature bone. It can be defined as the sum of two contributions representing cartilage and bone:

$$\alpha(\boldsymbol{x}, t) = \alpha_b(\boldsymbol{x}, t) + \alpha_c(\boldsymbol{x}, t) \tag{7}$$

where α_b corresponds to the contribution of bone formation to the mechanical properties of the fracture which is related to the amount of bone, and α_c corresponds to the contribution of cartilage formation. These variables represent the recovery of the mechanical properties of the fracture gap due to bone and cartilage formation in a point $\boldsymbol{x}$. Each point is associated to a reference volume, thus, this union degree could be associated in some way to the amount of cartilage or bone per unit of volume. The value of $\alpha(\boldsymbol{x}, t)$ is limited to a maximum of one. The temporal evolution of α at each point is driven by the maximum principal compression strain ε_n, the maximum distortion strain ε_{sh}, and the maturation time for each type of tissue:

$$\varepsilon_n(\boldsymbol{x}) = \varepsilon_{III} \tag{8}$$

$$\varepsilon_{sh}(\boldsymbol{x}) = \frac{\varepsilon_I - \varepsilon_{III}}{2} \tag{9}$$

where ε_I and ε_{III} are the maximum and minimum principal strains respectively. These stimuli as well as the maturation time define the evolution of the different tissues in the fracture gap. Three different healing zones (cf. Fig. 2-a) are defined:

- Zone 1: Non-union

Only fibrous tissue is formed due to high compression and shear strains, no bone or cartilage is formed:

$$\frac{\partial \alpha_c}{\partial t} = \frac{\partial \alpha_b}{\partial t} = 0. \tag{10}$$

- Zone 2: Cartilage formation

Moderate compression and shear strains lead to cartilage formation after a maturation time M_c. α_c will grow exponentially according to Fig. 2-b.

$$\frac{\partial \alpha_c}{\partial t} \geq 0, \frac{\partial \alpha_b}{\partial t} = 0. \tag{11}$$

- Zone 3: Bone formation

Low compression and shear strains lead to bone formation after a maturation time M_c. α_b will grow linearly according to Fig. 2-c.

$$\frac{\partial \alpha_c}{\partial t} = 0, \frac{\partial \alpha_b}{\partial t} \geq 0. \tag{12}$$

2.3. Numerical implementation

The pitting corrosion and bone healing algorithms have been implemented in Abaqus/Standard 6.14 (Dassault Systèmes, Waltham, MA, USA) by means of a UMAT subroutine. The flowchart of the subroutine is described in Fig. 1. Preprocessing was performed on the plates meshes using a Python script. The connectivity map of the elements was computed and a random value of λ was assigned to the surface elements to model the pits from which the corrosion spreads.

2.4. FE modelling of an orthognathic surgery case

The FE model presented here is based on a clinical orthognathic surgery case in which five osteotomies (two in the maxilla, two in the mandible and one in the chin) have been performed and fixed with patient-specific titanium plates. The patient is a 23-year-old female. Virtual planning has been used for this case (Proplan CMF, Materialise NV, Leuven, Belgium). A preoperative CT scan of the patient's head was performed. This CT scan has been segmented (Mimics v23, Materialise NV, Leuven, Belgium) in order to obtain 3D models of the patient's bones (maxilla, mandible). During a virtual planning session, the surgeon and a clinical engineer define the cutting planes for each osteotomy and the final configuration of the bone segments in order to achieve a complete occlusion.

The present work focuses on the bisagittal split osteotomy (BSSO), which consists of separating each ramus from the mandible during the surgery. Two plates were used to stabilize the fracture gap and no further treatment was applied to the patient. In this configuration, the plates have to undergo the masticatory load and are the most mechanically stressed, and the mechanical environment in the fracture gaps is mainly compressive. The FE model mesh is based on the final configuration of the bone segments of interest (mandible, left and right ramus, teeth). The rami and the mandible were overlapping so a 1 mm-thick fracture gap was defined at their interface.

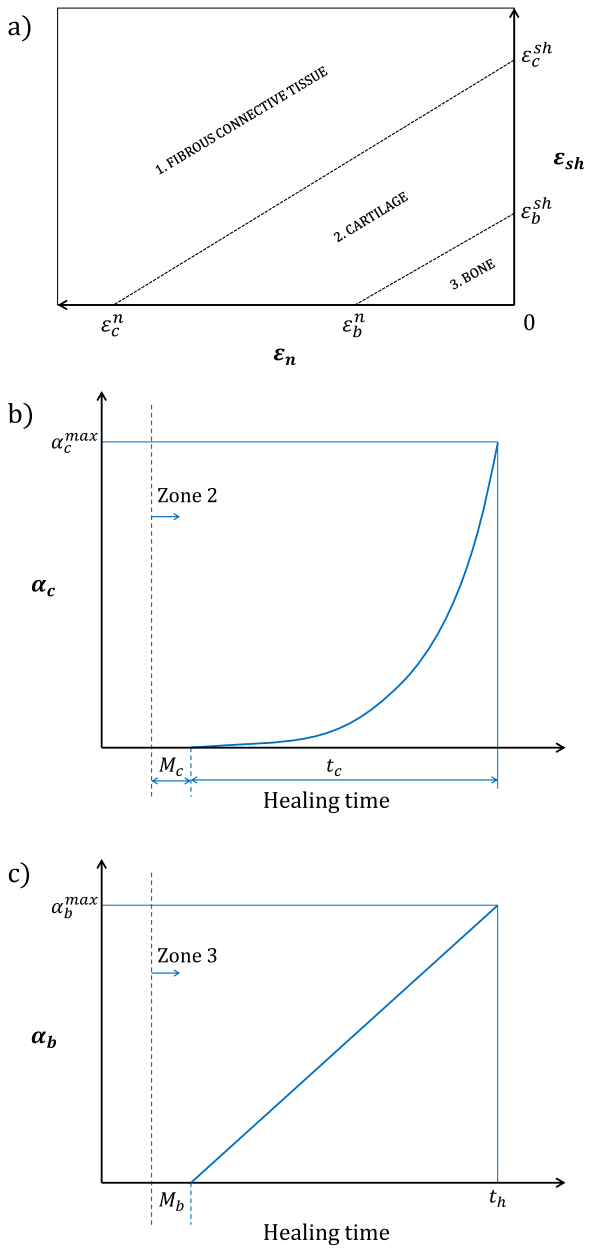

Fig. 2. (a) Healing zones, (b) temporal evolution of α_c and (c) temporal evolution of α_b; ε_b^{comp} and ε_c^{comp} are the compression strain limits for bone and cartilage formation respectively; ε_b^{sh} and ε_c^{sh} are the distortion strain limits for the formation of bone and cartilage respectively; M_c and M_b are the respective maturation times of cartilage and bone; t_c is the cartilage formation time and t_h is the total healing time.
Source: Reproduced from Alierta et al. (2014)

2.4.1. Plate design

For this clinical case, patient-specific titanium plate designs (SynpliciTi, Materialise NV, Leuven, Belgium) were generated from the final configuration of the bone segments. This first design (A) consists of titanium, which has higher mechanical strength (E_{Ti} = 110 Gpa) than Magnesium (E_{p0} = 44 Gpa). Thus, the design parameters (width and thickness) of this plate have been tuned to generate a second design (B) with a higher mechanical stiffness. These plate designs are presented in Fig. 3 and their design parameters are indicated in Table 2, as well as their specific surface area.

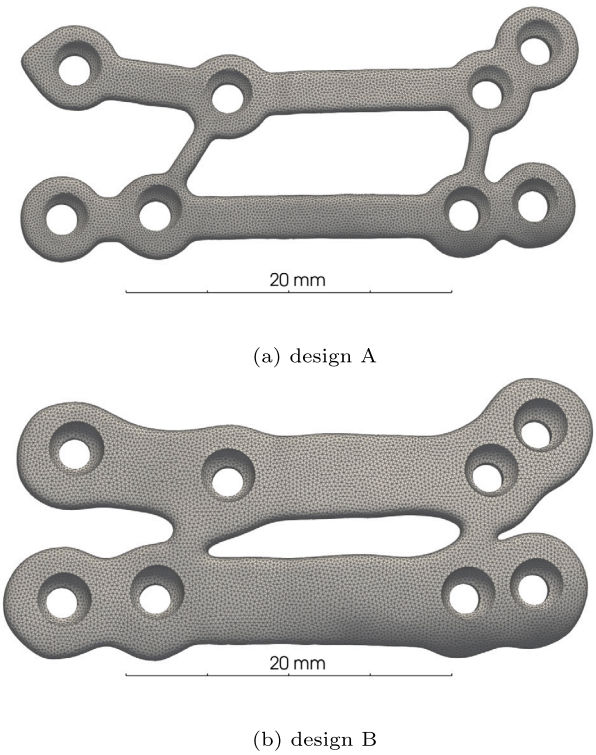

Fig. 3. Surface mesh of the right-side plate for each design.

2.4.2. Meshing

The parts of the model have been meshed with tetrahedral linear elements (C3D4) using 3-matic (v15.0 Materialise NV, Leuven, Belgium). For bony structures (mandible, rami, teeth), maximum edge length on the surface is 1.5 mm resulting in a total of approximately 540,000 linear tetrahedral elements and 108,000 nodes. The fracture gaps have been meshed with an element length of 1 mm, resulting in approximately 3500 elements and 1300 nodes in each gap. The plates are meshed with a maximum element length of 0.25 mm for the region comprised within 0.5 mm of the surface. The cores of the plates are meshed with a maximum element length of 0.5 mm. The two plates corresponding to design B entail approximately 1,180,000 elements and 205,000 nodes in total. A sensitivity analysis was performed to determine the mesh size of the plates after performing a sensitivity analysis based on evolution of the mass loss. The nodes are coincident at the interfaces between the bony structures and the fracture gaps.

2.4.3. Screw model

The screw model used here is described in more detail in the work of Pitocchi et al. (2020). The fixation screws tying the plates to the bone fragments are modelled as structural elements. 16 standard CMF screws are modelled (outer diameter = 2.5 mm, root diameter = 2 mm, 4 mm ≤ length ≤ 6 mm). Beam elements (B32, three-node) were used to mesh the screw wire. Rigid connectors were used to connect the wire with the nodes of the bone elements situated within the outer screw radius. The connection between the screw head and the plates is done in a similar way, with rigid connectors between the nodes corresponding to the screw head with the plates nodes situated within the screw head radius. Non-degradable titanium screws are considered for these simulations.

2.4.4. Material properties

Ground plates made of the WE43 magnesium alloy are considered and the values of the parameters are taken from the work of Boland

Table 1
Model parameters.

Parameter	Description	Value	Unit	Ref.
Pitting corrosion				
E_{p0}	Initial Young's modulus of magnesium	44	GPa	(Agarwal et al., 2016)
ν_p	Poisson's ratio of magnesiums	0.3	–	(Boland et al., 2018)
σ_{yield}	Magnesium's yield strength	0.3	GPa	(Agarwal et al., 2016)
k_U	Corrosion kinetic parameter	0.0003	day^{-1}	Estimated
β	Pit growth parameter	0.8	–	(Boland et al., 2018)
δ_U	Material characteristic length	0.015	mm	(Boland et al., 2018)
γ	Weibull distribution shape factor	0.2	–	(Boland et al., 2018)
Bone healing				
E_{g0}	Young's modulus of immature bone	1	GPa	(Lacroix and Prendergast, 2002)
ν_g	Poisson's ratio of the fracture gap	0.3	–	(Lacroix and Prendergast, 2002)
M_c	Maturation time for cartilage	4	days	(Alierta et al., 2014)
M_b	Maturation time for bone	10	days	(Alierta et al., 2014)
α_c^{max}	Maximum value of α_c	0.3	–	(Alierta et al., 2014)
α_c^{max}	Maximum value of α_b	0.7	–	(Alierta et al., 2014)
t_c	Cartilage formation time	36	days	(Alierta et al., 2014)
t_h	Total healing time	60	days	(Alierta et al., 2014)
ε_c^n	Compression strain limit for cartilage formation	10	%	(Perren and Rahn, 1980)
ε_b^n	Compression strain limit for bone formation	2	%	(Perren and Rahn, 1980)
ε_c^{sh}	Shear strain limit for cartilage formation	10	%	(Gómez-Benito et al., 2005)
ε_b^{sh}	Shear strain limit for bone formation	3	%	(Gómez-Benito et al., 2005)

Table 2
Design parameters of the bone plates: thickness and width of the cross-section; specific surface area (SSA).

Design	Thickness (mm)	Width (mm)	SSA (mm^2/mm^3)
A	1	2.6	2.93
B	1.5	4.6	1.88

Table 3
Mechanical properties of the materials used in the FE model.

Material	E (GPa)	ν	Parts
Bone	6	0.3	Mandible, rami
Teeth	14	0.3	Teeth
Titanium	110	0.37	Screws

Table 4
Distribution of the muscle force and unit vector coordinates for each muscle group during unilateral molar clenching.

Muscle group	Muscle forces (N)		Unit vector coordinates		
	WS[a]	BS[b]	X[c]	Y	Z
Superficial masseter	137.09	114.24	−0.207	−0.419	0.885
Deep masseter	58.75	48.96	−0.550	0.358	0.758
Lateral pterygoid	20.07	43.49	0.630	−0.757	−0.174
Medial pterygoid	146.83	104.88	0.486	−0.372	0.791
Anterior temporalis	115.34	91.64	−0.149	−0.044	0.988
Middle temporalis	63.10	64.05	−0.221	0.500	0.837
Posterior temporalis	44.60	29.48	−0.208	0.855	0.474

[a]WS = working side (right).
[b]BS = balancing side (left).
[c]Right side, opposite values have to be taken for the left side.

et al. (2018) (cf. Table 1). This study shows that grinding the specimens significantly slows down the corrosion process. The corrosion parameters for ground magnesium are only known for the uniform corrosion model. The parameter k_U for pitting corrosion has been estimated by fitting the mass loss over time with the uniform corrosion model. The maximum Young modulus of the fracture gaps corresponds to immature bone, the parameters of the bone healing algorithm are defined in Table 1. The other materials (bone, teeth, titanium) are assumed linear elastic materials and their mechanical properties are listed in Table 3.

2.4.5. Load definition and boundary conditions

The mastication loads have been modelled by considering unilateral molar clenching. Left and right clenching are simulated successively for a time period of one day. Thus, the displacement along the z-axis is blocked alternatively on the first molar of the working side (cf. Fig. 4-a). The condyles centres are blocked in all directions, and the muscle forces are applied on the areas corresponding to the respective muscles (Table 4).

The distribution of the physiological muscle forces are taken from Korioth et al. (1992), based on a healthy subject. However, a patient cannot bite at full force during the post-operative period due to the soft tissues and bone healing processes. The calculation of the fraction of the physiological load applied to the system is based on Ohkura et al. (2001). In this study, the maximum bite force has been measured on a cohort of patients at several time points after an orthognathic surgery. The physiological load fraction has been defined from this data such that the maximum bite force at a given time point normalized to the maximum bite force 3 years after the operation. This ratio was computed at 15, 30 and 90 days after the operation. A linear interpolation was done to estimate the load fraction for each day of the healing period, as it is represented on Fig. 4-b.

2.4.6. Post-processing FE output

Five variables are defined to characterize the global evolution of the system over time. The bone healing process is described by the average union degree ($\overline{\alpha}$), the average value of (α) in both fracture gaps weighted by the element volumes. It is the sum of $\overline{\alpha}_b$ and $\overline{\alpha}_c$, the respective contributions of bone and cartilage formation to the healing. The relative mass loss resulting of corrosion, $(m_i - m(t))/m_i$ with m_i being the initial mass of the plates and $m(t)$ their mass at a given time. It is determined by computing the average value of the damage (D) in the plates weighted by the element volumes. The maximum value of the Von Mises (VM) stress (σ_{VM}^{max}) represents the mechanical resistance of the plate at a given time. In order to avoid numerical singularities, it is equal to the average VM stress in the 20 elements with highest values. The mechanical state of the plate is defined via the ratio $\sigma_{VM}^{max}/\sigma_{yield}$, σ_{yield} being the yield strength of the material.

The computations were performed using Abaqus/Standard 6.14 (Dassault Systèmes, Waltham, MA, USA) with 5 Intel Xeon CPUs and 40 GB of RAM allocated to each simulation. The computational time of the model for design B was 93,500 s.

3. Results

The evolution of the variables defined to characterize the system (mass loss, maximum VM stress, healing union degree) is illustrated

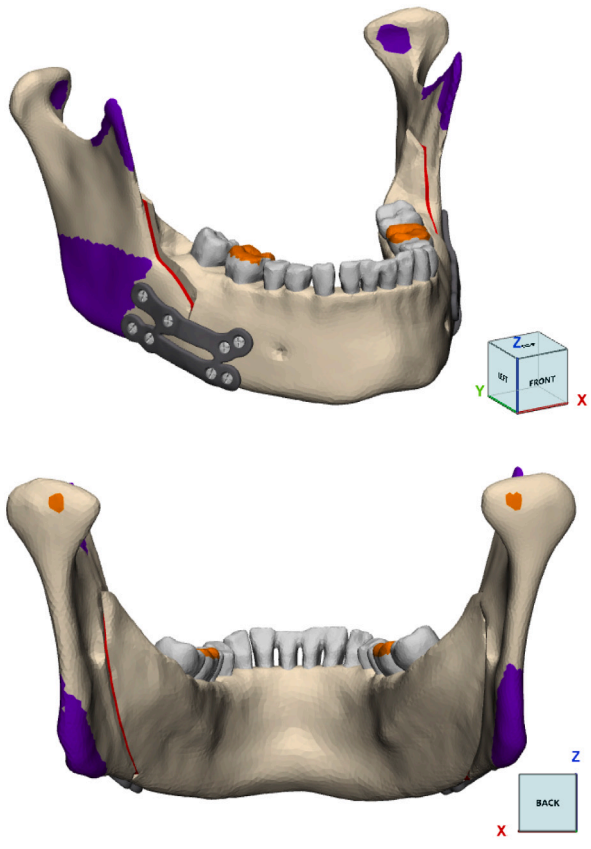

(a)

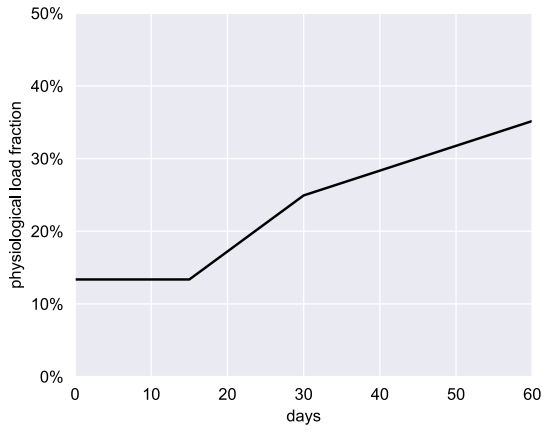

(b)

Fig. 4. (a) Boundary conditions applied on the patient-specific model: fracture gaps (red), muscle insertions (purple) and fixed displacement (orange) in all three directions at the centre of the condyles and along the z-axis for the molars (b) fraction of the physiological load of a healthy subject applied on the mandible during the period of interest.

in Fig. 5 for each design. The relative mass loss is higher in the case of design A due to the higher specific surface area (cf. Table 2). Pitting corrosion of magnesium is a surface phenomenon, hence the higher the specific surface area, the higher the relative mass loss. The maximum VM stress at the beginning of the simulation is higher for design A (≈ 90% of σ_{yield}) than for design B (≈ 40% of σ_{yield}).

Bone healing and pitting corrosion have adverse effects on the VM stress, the formation of bone leads to a higher load transmission in the fracture gaps while the mass loss caused by corrosion decreases the mechanical integrity of the plates. In a first phase – up to 40 days for design A and up to 20 days for design B – the effect of bone formation is prevalent and the maximum VM stress in the plates is decreasing. In a second phase, the degradation has more effect and the maximum von Mises stress increases steadily. In the case of design B, the maximum von Mises stress is comprised between 20 and 40% of the yield strength which can be considered stable.

The evolution of the system for design B is illustrated in Fig. 6. Corrosion pits are present on the surface of the plates, some of them being present around the screw holes. The distribution of these pits is similar to what can be observed experimentally for ground Mg in the study of Boland et al. (2018). A stress concentration can be observed around the pits, as the cross-section is reduced locally (see the plate cross-section at 61 days in Fig. 6).

At the end of the simulation the value of the healing union degree ($\overline{\alpha}$), which is proportional to the Young modulus of the fracture gaps, is inferior for design B than for design A (cf. Fig. 5). This can be attributed to less cartilage formation for the alternative design, as bone formation was similar for both designs.

4. Discussion

The results of this study show the feasibility to compare the performance of two different plate designs using a time-dependent model. The superior stiffness of the design B plates results from their larger dimensions, while the design A plates might not be able to withstand the mastication loads just after the surgery. As shown on Fig. 6, it is possible that this design would fail at day 1 if magnesium is used. It shows that new designs need to be developed for this material. Design B is thicker and exhibits a better mechanical resistance to the masticatory loads exerted on the plates. However, it has been shown that bone healing could be inhibited by a very stiff plate (Chandra and Pandey, 2020). Therefore, the plate stiffness must be tuned to ensure its mechanical integrity and promote the fracture healing process at the same time.

The results show that changing the plate design has an effect on the bone healing process. The union degree of the fracture gaps, hence the stiffness of the gap, is lower when design B is used. We can see in Fig. 6 that 61 days after the surgery, the bone healing is not completely homogeneous in the right gap as the union degree is not 100% in the full gap. Cartilage formation is almost three times more important for design A ($\overline{\alpha}_c$ = 23%) than for design B ($\overline{\alpha}_c$ = 8%) (cf. Fig. 5). We can consider that for design A endochondral ossification was predominant as both bone and cartilage were formed. On the other hand, intramembranous ossification was predominant for design B as the proportion of cartilage formed is low. As design A is more flexible, the interfragmentary strain in the fracture gaps is higher. Cartilage formation requires higher stimulus (cf. Fig. 2-a) so it could be inhibited if the fixation system is too stiff. This is consistent with what has been highlighted in the literature (Hak et al., 2010; Bartnikowski et al., 2017), i.e that a flexible fixation promotes bone regeneration. From a clinical perspective, this means that an ideal plate design would consist of biodegradable plates exhibiting a slowly decreasing mechanical strength, thereby increasing progressively the interfragmentary strain in the callus. This high mechanical stimulus would promote intramembranous ossification, resulting in higher callus stiffness. On the contrary, using a very stiff plate could inhibit this healing process. In addition, a very thin design could lead to a fast degradation and an early failure of the plates. A balance must be found to attain maximum callus stiffness at the end while maintaining the mechanical integrity of the plate.

The bone healing model of Alierta et al. (2014) was developed for fractures of reduced thickness in long bones using cohesive elements. We generalized this formulation to 3D solid mechanics elements,

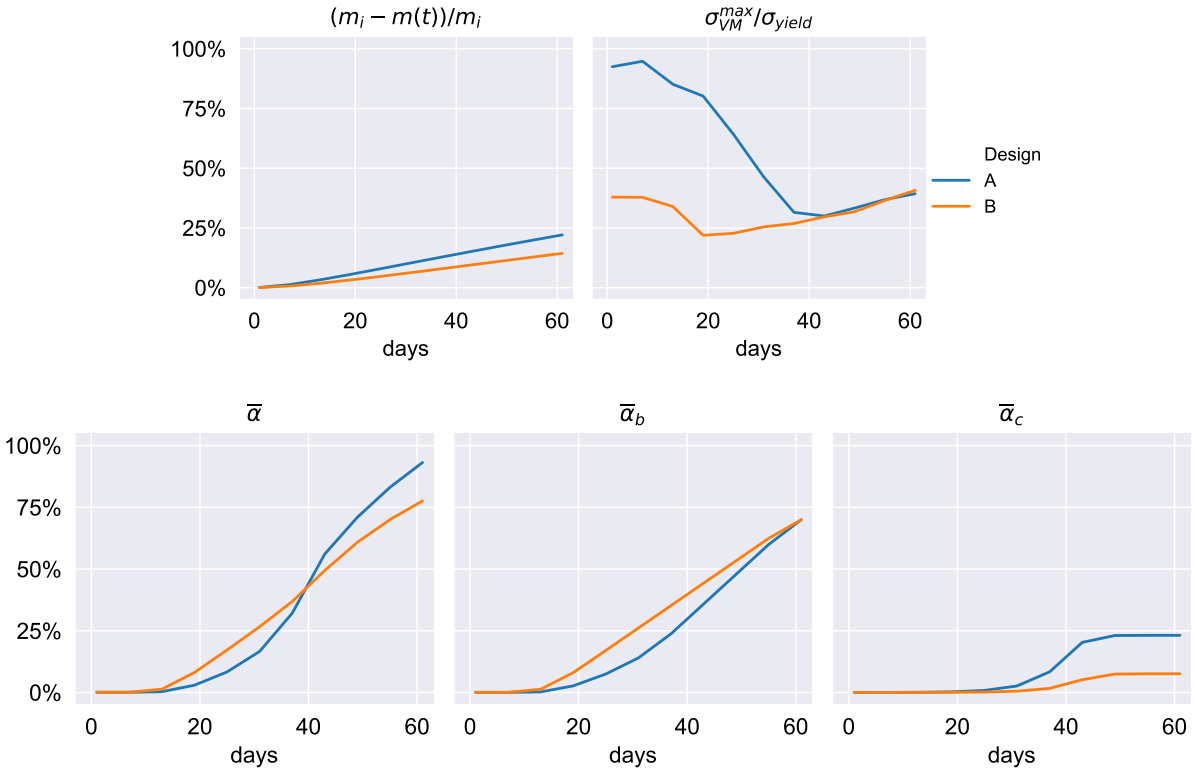

Fig. 5. Evolution of (from left to right and top to bottom): the relative mass loss ($(m_i - m(t))/m_i$) and maximum VM stress (normalized by the yield strength of Mg) ($\sigma_{VM}^{max}/\sigma_{yield}$) in the plates; the fracture gaps average healing union degree ($\overline{\alpha}$) for each design through the healing period and the average bone ($\overline{\alpha}_b$) and cartilage ($\overline{\alpha}_c$) formation for each design through the healing period.

therefore it can be used for more complex fracture geometries. There was an overlap of the bones in the clinical case studied here, but fracture gaps can be irregular in other orthognathic surgery cases. Thus, the bone healing model presented here could be applied to these irregular fracture gaps. Boccaccio et al. (2008) used a tissue-level bone algorithm to simulate mandibular distraction. This model provides details of the healing process at the tissue scale simulating the events occurring at the fracture callus. Cell migration is considered and tissue differentiation was driven by octahedral shear strain and fluid flow, contrary to the model presented here where compressive and shear strains are used. The results of Boccaccio et al. show that masticatory loads promote osteogenesis, which coincides with what is observed in the present study. A bone healing algorithm with a simpler mathematical formulation has been used in the present work to reduce the computational cost of the FE model as two subroutines are used. We do not simulate a detailed description of the events occurring at the fracture callus, however we represent the healing outcome by one variable representing the structural integrity of the fracture gap. The aim is to provide a tool able to assist in the preoperative planning of BSSO with magnesium plates avoiding complex and time-consuming simulations.

To perform our simulations, several simplifications were needed. Firstly, the fixation system was simplified as no pre-tightening force between the plate and the bone was modelled, which does not correspond to what is done clinically. The pre-tightening force was not modelled to reduce the computational cost of the model. It represents a worst-case situation for the plates as the load is entirely transmitted through the screws. However, as a next step, the workflow presented here can be adapted to model this pre-tightening force. The other simplifications made on the fixation (non-degradable screws and 2D beam elements) and the mass loss that can be observed around the screw holes (Fig. 7) suggest that fixation failure could happen. Therefore, further research focusing on this aspect would be needed to develop biodegradable fixation systems.

Secondly, the corrosion algorithm used here is calibrated with *in vitro* corrosion experiments. However, the *in vitro* and *in vivo* corrosion rates can drastically differ due to multiple factors (Kirkland and Birbilis, 2014) such as the chemical environment, the alloy composition, the implant location in the body and surface treatment. The *in vitro* corrosion rate of ground Mg is lower than for untreated Mg but it is not possible to affirm that it would be the same *in vivo*. It would be necessary to conduct further *in vivo* testing to get a better estimation of the degradation rate for this type of applications. This corrosion algorithm could be modified to evaluate other biodegradable metals such as Zn-based alloys and Fe-based alloys. Zn-based alloys were not considered here because of their lower mechanical properties compared to magnesium. The slower degradation rates of Fe-based alloys make them less suitable for our model, as the risk of early failure is much lower (Shuai et al., 2019).

Thirdly, the results of Ohkura et al. (2001) show that there is a high variability on the modulus of masticatory loads between patients. In this model we assumed standard values from the literature (Korioth et al., 1992) and that the activation of the different muscles was uniform when a fraction of the load was applied. The use of musculoskeletal models is a potential answer to this need of personalization. Such models have been developed for the mandible (de Zee et al., 2007; Skipper Andersen et al., 2017) and could be used in the framework of a clinical study on patients during the healing period in order to have a better understanding of the loads applied on the mandible in this context. In addition, biting was simplified by fixing the displacement of the first molar, rather than applying the biting force. As to the best of our knowledge there is no literature that describes the full

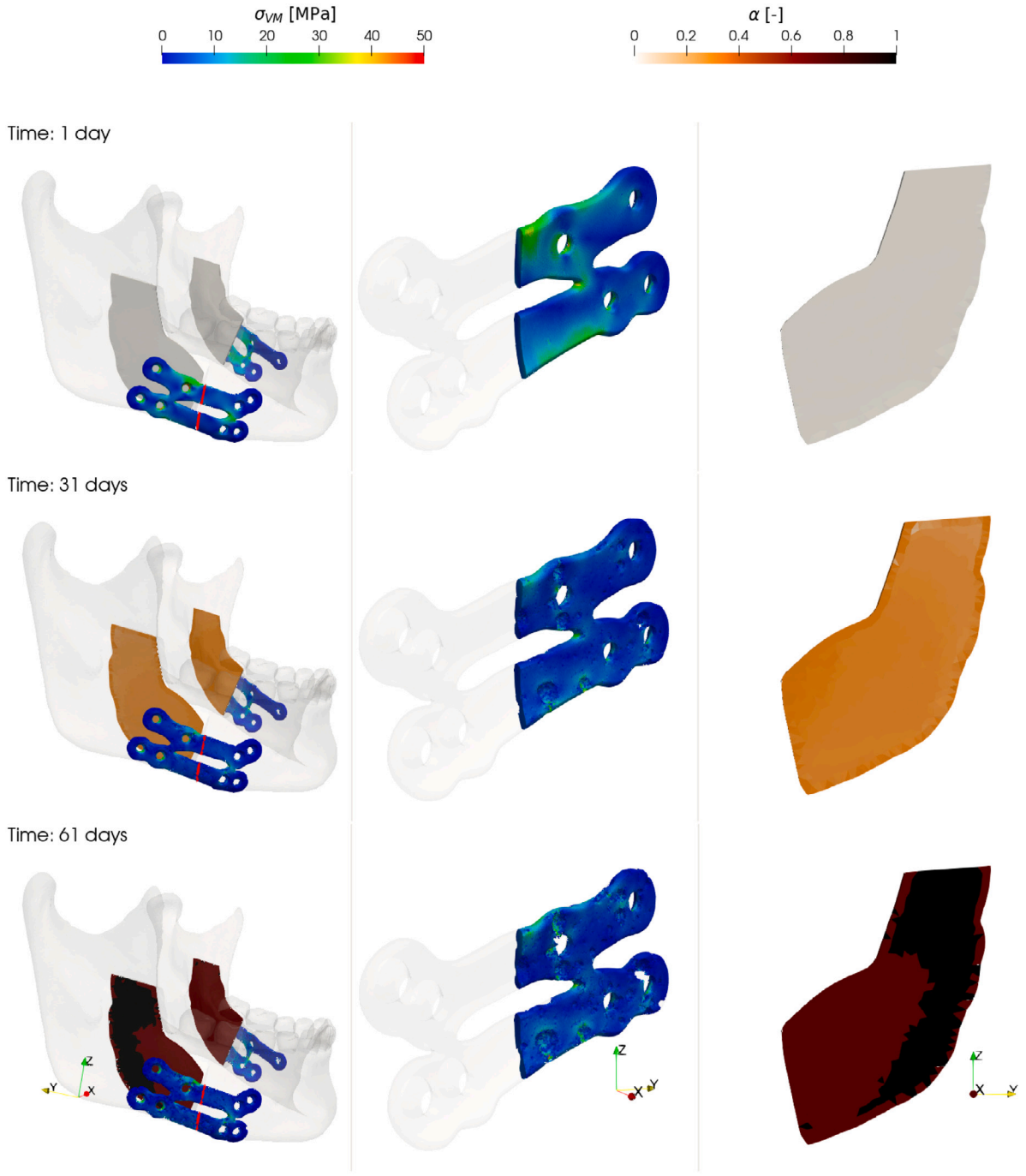

Fig. 6. From left to right: isometric view of the mandible, cut view of the right plate cross-section and side view of the right bone gap after 1, 31 and 61 days for plate design B. The distributions of the bone healing union degree α and of the VM stress σ_{VM} are represented respectively on the fracture gaps and the plates. The cross-section is represented by the red line on the isometric view.

physiological loading conditions (i.e. muscle and biting forces on the individual teeth), we did not have a consistent dataset to apply all forces to the model and therefore simplified the displacement of the first molar. These elements show that further investigation is needed in order to increase the reliability of its predictions.

Finally, only the first phase of the recovery is simulated in this model. A complete healing (α = 1) after 60 days corresponds to the formation of immature bone (E = 1 GPa). It is less stiff than the surrounding mature bone (E = 6 GPa), so the union is not perfect. Therefore, a bone remodelling algorithm would be needed to simulate the complete healing of the fracture.

In conclusion, the model developed in this study was able to estimate the evolution of biodegradable CMF bone plates by simulating the evolution of the system comprising the mandible and the bone plates after an orthognathic surgery. The aim of this study was to determine the feasibility of creating a clinically feasible workflow, and the next step is to further validate the model in a clinical population. Bone healing and biodegradation algorithms were incorporated to take into account the

(a) design A

(b) design B

Fig. 7. Comparison of the degradation after 61 days in the right plate of each design.

two phenomena influencing dynamically the mechanical state of the system over time. This time-dependent approach is necessary due to the evolving mechanical strength of bioresorbable plates. The methodology described here could be applied to other orthognathic surgery cases (including worst-case scenarios) to gain more insights into the design of biodegradable plates. The workflow presented in this paper offers a model of healing at the organ level, thereby providing a model in which all the healing is considered following the seminal work of Perren and Rahn (1980).

CRediT authorship contribution statement

Antoine Vautrin: Concept, Design, Methodology, Software, Investigation, Analysis, Writing, Revision of the manuscript. **Mariska Wesseling:** Concept, Analysis, Supervision, Revision of the manuscript. **Roel Wirix-Speetjens:** Concept, Analysis, Supervision, Revision of the manuscript. **Maria Jose Gomez-Benito:** Concept, Methodology, Analysis, Supervision, Revision of the manuscript.

Declaration of competing interest

The authors declare that they have no known competing financial interests or personal relationships that could have appeared to influence the work reported in this paper.

Funding

This project has received funding from the European Union's Horizon 2020 Research and Innovative program under the Marie Skłodowska-Curie grant agreement No 722535.

References

Agarwal, S., Curtin, J., Duffy, B., Jaiswal, S., 2016. Biodegradable magnesium alloys for orthopaedic applications: A review on corrosion, biocompatibility and surface modifications. Mater. Sci. Eng.: C 68, 948–963. http://dx.doi.org/10.1016/j.msec.2016.06.020.

Alierta, J., Pérez, M., García-Aznar, J., 2014. An interface finite element model can be used to predict healing outcome of bone fractures. J. Mech. Behav. Biomed. Mater. 29, 328–338. http://dx.doi.org/10.1016/j.jmbbm.2013.09.023.

Bartnikowski, N., Claes, L.E., Koval, L., Glatt, V., Bindl, R., Steck, R., Ignatius, A., Schuetz, M.A., Epari, D.R., 2017. Modulation of fixation stiffness from flexible to stiff in a rat model of bone healing. Acta. Orthop. 88 (2), 217–222. http://dx.doi.org/10.1080/17453674.2016.1256940.

Boccaccio, A., Prendergast, P.J., Pappalettere, C., Kelly, D.J., 2008. Tissue differentiation and bone regeneration in an osteotomized mandible: a computational analysis of the latency period. Med. Biol. Eng. Comput. 46 (3), 283–298. http://dx.doi.org/10.1007/s11517-007-0247-1.

Boland, E.L., Shirazi, R.N., Grogan, J.A., McHugh, P.E., 2018. Mechanical and corrosion testing of magnesium WE43 specimens for pitting corrosion model calibration. Adv. Eng. Mater. 20 (10), 1800656. http://dx.doi.org/10.1002/adem.201800656.

Borgiani, E., Duda, G.N., Checa, S., 2017. Multiscale modeling of bone healing: Toward a systems biology approach. Front. Physiol. 8, 287. http://dx.doi.org/10.3389/fphys.2017.00287.

Buijs, G., van Bakelen, N., Jansma, J., de Visscher, J., Hoppenreijs, T., Bergsma, J., Stegenga, B., Bos, R., 2012. A randomized clinical trial of biodegradable and titanium fixation systems in maxillofacial surgery. J. Dent. Res. 91 (3), 299–304. http://dx.doi.org/10.1177/0022034511434353.

Byun, S.-H., Lim, H.-K., Cheon, K.-H., Lee, S.-M., Kim, H.-E., Lee, J.-H., 0000. Biodegradable magnesium alloy (WE43) in bone-fixation plate and screw, p. 8.

Chandra, G., Pandey, A., 2020. Biodegradable bone implants in orthopedic applications: a review. Biocybern. Biomed. Eng. 40 (2), 596–610. http://dx.doi.org/10.1016/j.bbe.2020.02.003.

Gastaldi, D., Sassi, V., Petrini, L., Vedani, M., Trasatti, S., Migliavacca, F., 2011. Continuum damage model for bioresorbable magnesium alloy devices — Application to coronary stents. J. Mech. Behav. Biomed. Mater. 4 (3), 352–365. http://dx.doi.org/10.1016/j.jmbbm.2010.11.003.

Gómez-Benito, M., García-Aznar, J., Kuiper, J., Doblaré, M., 2005. Influence of fracture gap size on the pattern of long bone healing: a computational study. J. Theoret. Biol. 235 (1), 105–119. http://dx.doi.org/10.1016/j.jtbi.2004.12.023.

Gómez-Benito, M.J., García-Aznar, J.M., Kuiper, J.H., Doblaré, M., 2006. A 3D computational simulation of fracture callus formation: Influence of the stiffness of the external fixator. J. Biomech. Eng. 128 (3), 290–299. http://dx.doi.org/10.1115/1.2187045.

Grogan, J., O'Brien, B., Leen, S., McHugh, P., 2011. A corrosion model for bioabsorbable metallic stents. Acta Biomater. 7 (9), 3523–3533. http://dx.doi.org/10.1016/j.actbio.2011.05.032.

Hak, D.J., Toker, S., Yi, C., Toreson, J., 2010. The influence of fracture fixation biomechanics on fracture healing. In: Stahel, P.F. (Ed.), Orthopedics 33 (10), 752–755. http://dx.doi.org/10.3928/01477447-20100826-20.

Kirkland, N.T., Birbilis, N., 2014. Magnesium Biomaterials. In: SpringerBriefs in Materials, Springer International Publishing, http://dx.doi.org/10.1007/978-3-319-02123-2.

Korioth, T.W.P., Romilly, D.P., Hannam, A.G., 1992. Three-dimensional finite element stress analysis of the dentate human mandible. Am. J. Phys. Anthropol. 88 (1), 69–96. http://dx.doi.org/10.1002/ajpa.1330880107.

Lacroix, D., Prendergast, P., 2002. A mechano-regulation model for tissue differentiation during fracture healing: analysis of gap size and loading. J. Biomech. 35 (9), 1163–1171. http://dx.doi.org/10.1016/S0021-9290(02)00086-6.

Ma, S., Zhou, B., Markert, B., 2018. Numerical simulation of the tissue differentiation and corrosion process of biodegradable magnesium implants during bone fracture healing. Z. Angew. Math. Mech. 98 (12), 2223–2238. http://dx.doi.org/10.1002/zamm.201700314.

Mehboob, H., Chang, S.-H., 2015. Optimal design of a functionally graded biodegradable composite bone plate by using the taguchi method and finite element analysis. Compos. Struct. 119, 166–173. http://dx.doi.org/10.1016/j.compstruct.2014.08.029.

Naran, S., Steinbacher, D.M., Taylor, J.A., 2018. Current concepts in orthognathic surgery. Plast. Reconstr. Surg. 141 (6), 925e–936e. http://dx.doi.org/10.1097/PRS.0000000000004438.

Ohkura, K., Harada, K., Morishima, S., Enomoto, S., 2001. Changes in bite force and occlusal contact area after orthognathic surgery for correction of mandibular prognathism. Oral Surg. Oral Med. Oral Pathol. Oral Radiol. Endod. 91 (2), 141–145. http://dx.doi.org/10.1067/moe.2001.112334.

Perren, S.M., 2002. Evolution of the internal fixation of long bone fractures. The scientific basis of biological internal fixation: choosing a new balance between stability and biology. J. Bone. Joint Surg. British volume 84-B (8), 1093–1110. http://dx.doi.org/10.1302/0301-620X.84B8.0841093.

Perren, S.M., Rahn, B.A., 1980. Biomechanics of fracture healing. Can. J. Surg. 23 (3), 228–232.

Pitocchi, J., Wesseling, M., van Lenthe, G.H., Pérez, M.A., 2020. Finite element analysis of custom shoulder implants provides accurate prediction of initial stability. Mathematics 8 (7), 1113. http://dx.doi.org/10.3390/math8071113.

Schouman, T., Murcier, G., Goudot, P., 2015. The key to accuracy of zygoma repositioning: Suitability of the SynpliciTi customized guide-plates. J. Cranio-Maxillofac. Surg. 43 (10), 1942–1947. http://dx.doi.org/10.1016/j.jcms.2014.12.014.

Shuai, C., Li, S., Peng, S., Feng, P., Lai, Y., Gao, C., 2019. Biodegradable metallic bone implants. Mater. Chem. Front. 3 (4), 544–562. http://dx.doi.org/10.1039/C8QM00507A.

Skipper Andersen, M., de Zee, M., Damsgaard, M., Nolte, D., Rasmussen, J., 2017. Introduction to force-dependent kinematics: Theory and application to mandible modeling. J. Biomech. Eng. 139 (9), 091001. http://dx.doi.org/10.1115/1.4037100.

Sukegawa, S., Kanno, T., Manabe, Y., Matsumoto, K., Sukegawa-Takahashi, Y., Masui, M., Furuki, Y., 2018. Is the removal of osteosynthesis plates after orthognathic surgery necessary? Retrospective long-term follow-up study. Int. J. Oral and Maxillofac. Surg. 47 (12), 1581–1586. http://dx.doi.org/10.1016/j.ijom.2018.07.001.

Venugoplan, S.R., Nanda, V., Turkistani, K., Desai, S., Allareddy, V., 2012. Discharge patterns of orthognathic surgeries in the United States. J. Oral Maxillofac. Surg. 70 (1), e77–e86. http://dx.doi.org/10.1016/j.joms.2011.09.030.

Wu, C., Zheng, K., Fang, J., Steven, G.P., Li, Q., 2020. Time-dependent topology optimization of bone plates considering bone remodeling. Comput. Methods Appl. Mech. Engrg. 359, 112702. http://dx.doi.org/10.1016/j.cma.2019.112702.

de Zee, M., Dalstra, M., Cattaneo, P.M., Rasmussen, J., Svensson, P., Melsen, B., 2007. Validation of a musculo-skeletal model of the mandible and its application to mandibular distraction osteogenesis. J. Biomech. 40 (6), 1192–1201. http://dx.doi.org/10.1016/j.jbiomech.2006.06.024.

Zhao, F., Mc Garrigle, M.J., Vaughan, T.J., McNamara, L.M., 2018. In silico study of bone tissue regeneration in an idealised porous hydrogel scaffold using a mechano-regulation algorithm. Biomech. Model. Mechanobiol. 17 (1), 5–18. http://dx.doi.org/10.1007/s10237-017-0941-3.

Zheng, K., Liao, Z., Yoda, N., Fang, J., Chen, J., Zhang, Z., Zhong, J., Peck, C., Sasaki, K., Swain, M.V., Li, Q., 2019. Investigation on masticatory muscular functionality following oral reconstruction – An inverse identification approach. J. Biomech. 90, 1–8. http://dx.doi.org/10.1016/j.jbiomech.2019.04.007.